Supporting Information

for

Redox-assisted Multicomponent Deposition of Ultrathin Amorphous Metal Oxides on Arbitrary Substrates: Highly Durable Cobalt Manganese Oxyhydroxide for Efficient Oxygen Evolution

Ren-Huai Jhang, Chang-Ying Yang, Ming-Chi Shih, Jing-Qian Ho, Ya-Ting Tsai, and Chun-Hu Chen*

Department of Chemistry, National Sun Yat-sen University, Kaohsiung, Taiwan 80424

E-mail: chunhu.chen@mail.nsysu.edu.tw

Figure S-1: The EDXS results of $CMOH_{acetate}$. (a) The SEM images of CMOH with the selected area highlighted by red dashed lines for mapping analysis. (b) The EDXS results show the signals of Co and Mn with the atomic ratios of Co/Mn=3.08. The mapping results of Co (c) and Mn (d) distribution are shown in red and green, respectively, corresponding to the dashed line area in (a).

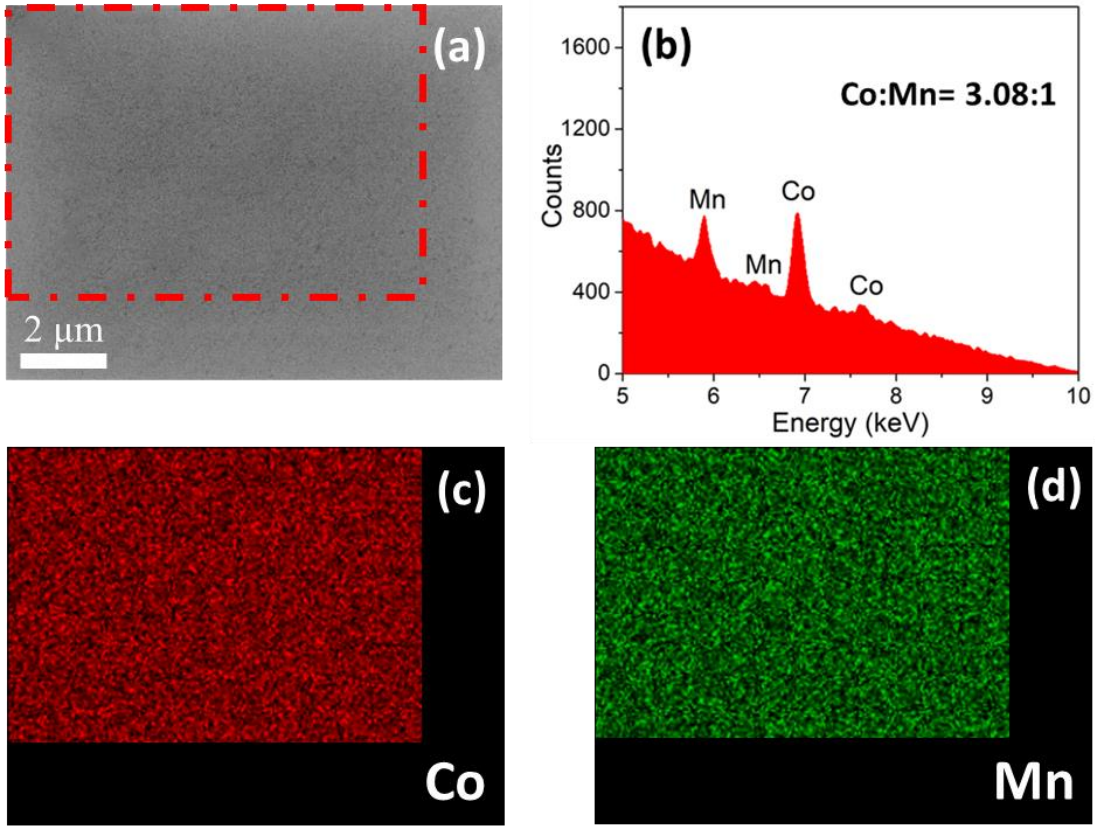

Figure S-2: The Raman spectra of CMOH show a broad band at 599 cm^{-1}, indicating the presence of amorphous cobalt oxide. The Raman signals of crystalline Co_3O_4 are shown for comparison.

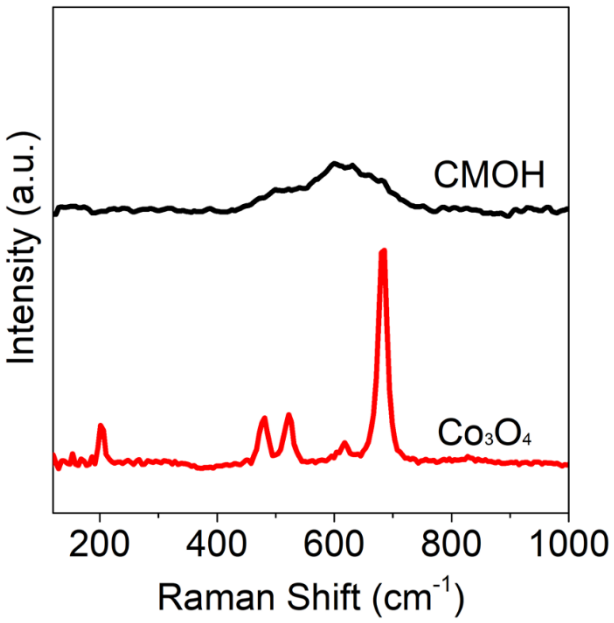

Figure S-3: The GIXRD pattern of the $CMOH_{sulfate}$ after calcination at 500°C, showing the phases corresponding to Co_3O_4.

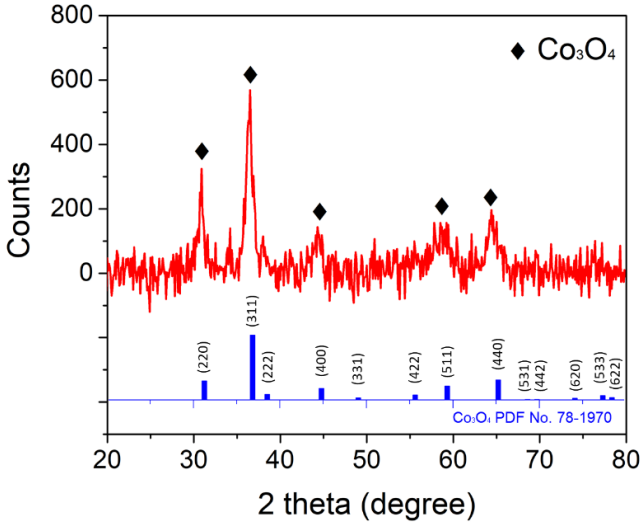

Figure S-4: The characterization of $CMOH_{acetate}$ cross-section under HR-TEM (also see Fig. 1g of the article). The label of **I** in the film area shows the EDXS signals with the majority of Co and Mn. The upper left inset shows the FFT patterns of **I** corresponding to an amorphous characteristic. The area labeled by **II** of FTO exhibits the strong Sn signal. The corresponding high resolution TEM images (the lower right inset) show a lattice corresponding to (110) of FTO. Ga signal is due to the ion-beam of Ga in FIB.

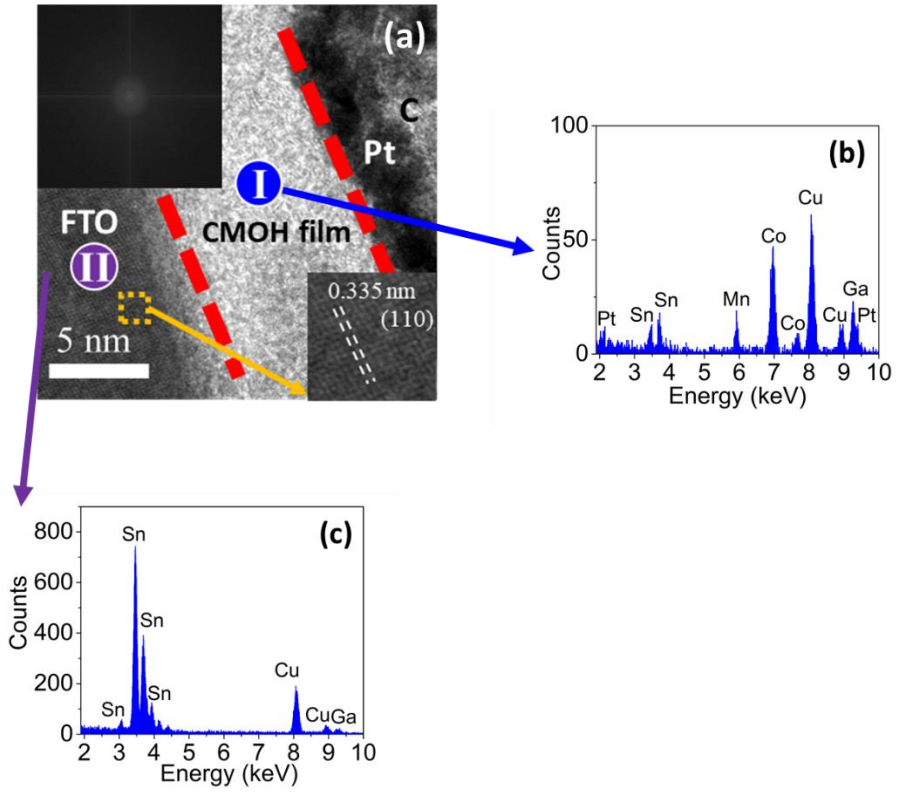

Figure S-5: AFM results of $CMOH_{acetate}$ show the film thickness around 11 nm prepared at 80ºC for 60 min.

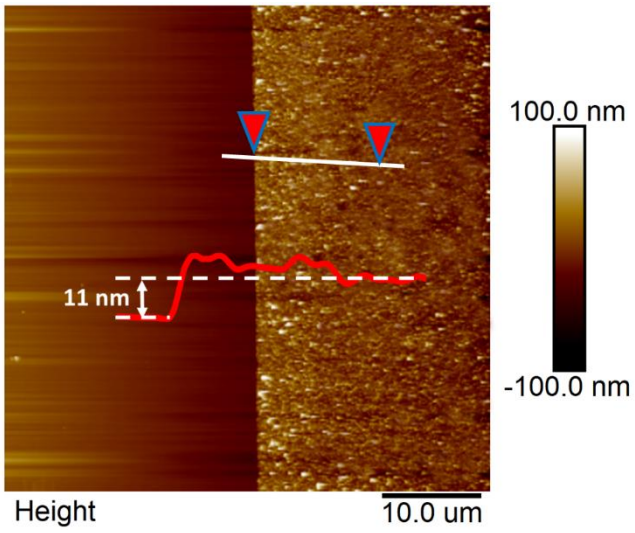

Figure S-6: The XPS data of the crystalline $CMO_{acetate}$ after annealing at 500℃. (a) Co 2p, (b) Mn 2p, and (c) O 1s.

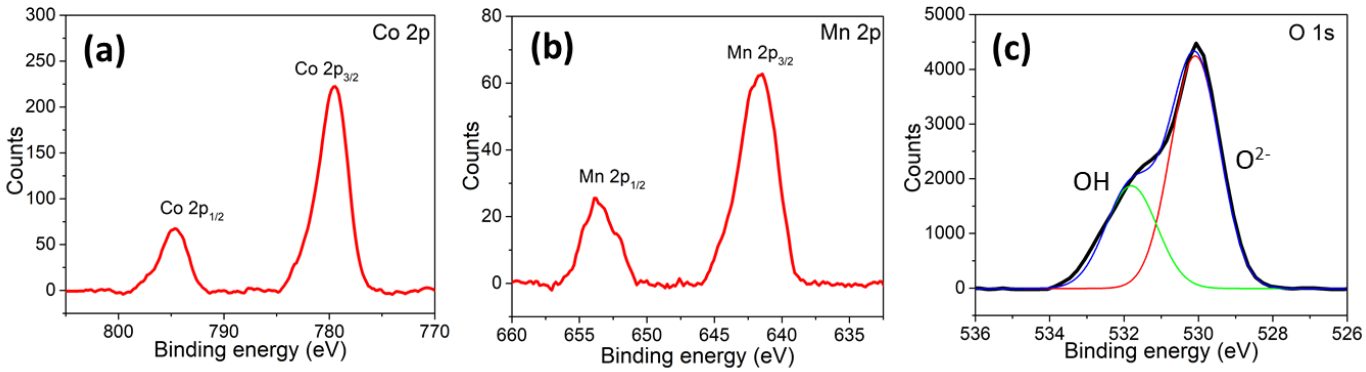

Figure S-7: The photographs of $Co(OAc)_2$-only and $KMnO_4$-only deposition on non-mental substrates of wood (a) and PET (b). The red arrows in (a) indicate the boundary between deposition and deposition-free areas for comparison. These results show no film formation by $Co(OAc)_2$-only deposition, while thin coating can be observed by $KMnO_4$-only deposition.

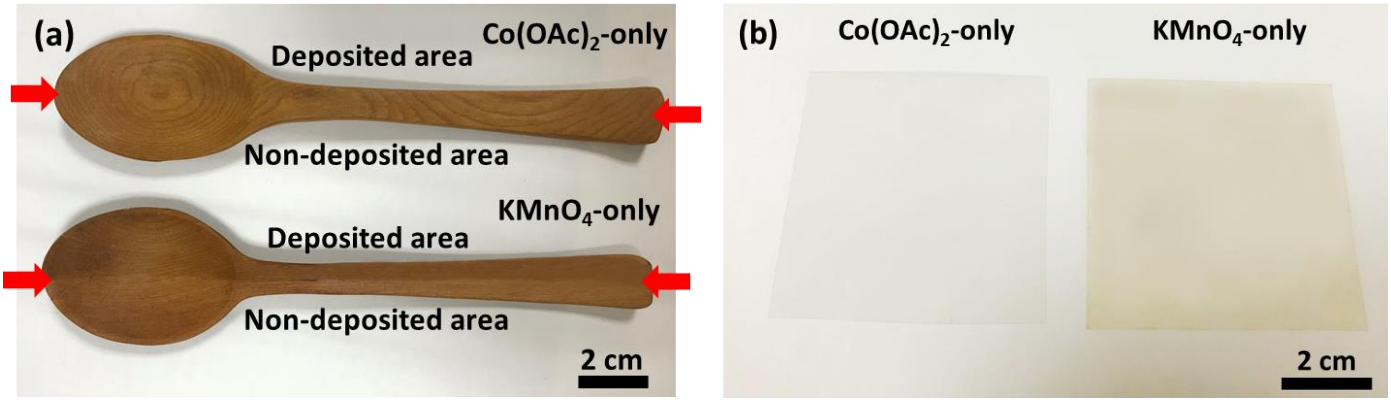

Figure S-8: Faradaic efficiency test of $CMOH_{acetate}$ films. After four hours oxygen evolution, the films exhibit the Faradaic efficiency of nearly 100%.

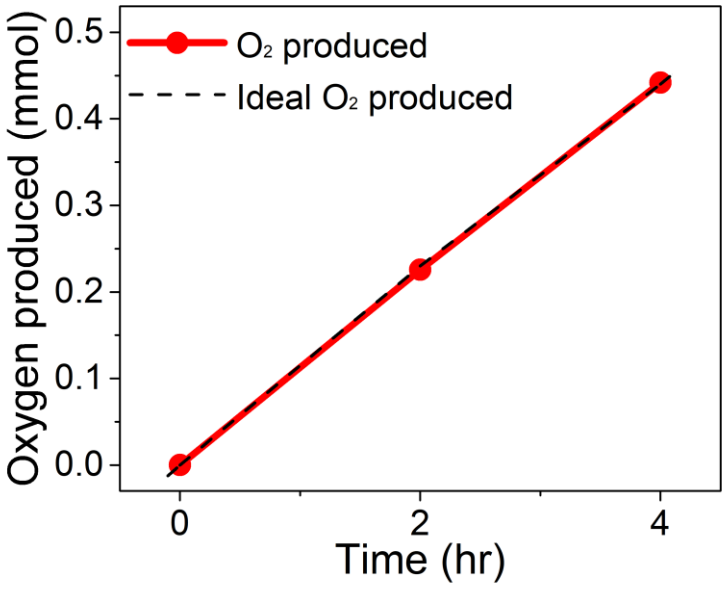

Figure S-9: The Tafel plots of $CMOH_{acetate}$ samples prepared by different Co/Mn precursor ratios at 80°C for 15 min. The Tafel slopes are summarized in the following table.

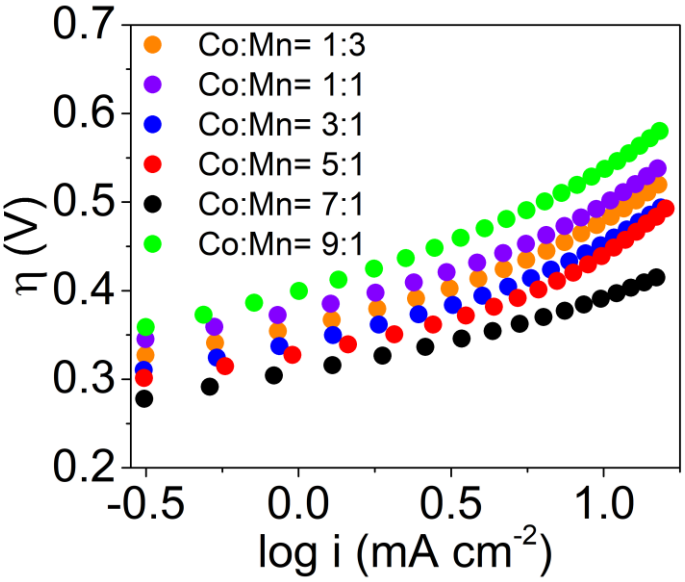

Sample	Tafel slope (mV/dec)
Co:Mn= 1:3	64.0
Co:Mn= 1:1	62.9
Co:Mn= 3:1	62.0
Co:Mn= 5:1	61.2
Co:Mn= 7:1	60.9
Co:Mn= 9:1	77.8

Figure S-10: The cobalt XPS data of the $CMOH_{7/1}$ (Co/Mn precursor ratio of 7/1) shows the high similarity to $CMOH_{3/1}$ (Co/Mn precursor ratio of 3/1), indicating that Co^{3+} is still the main species of the CMOH film.

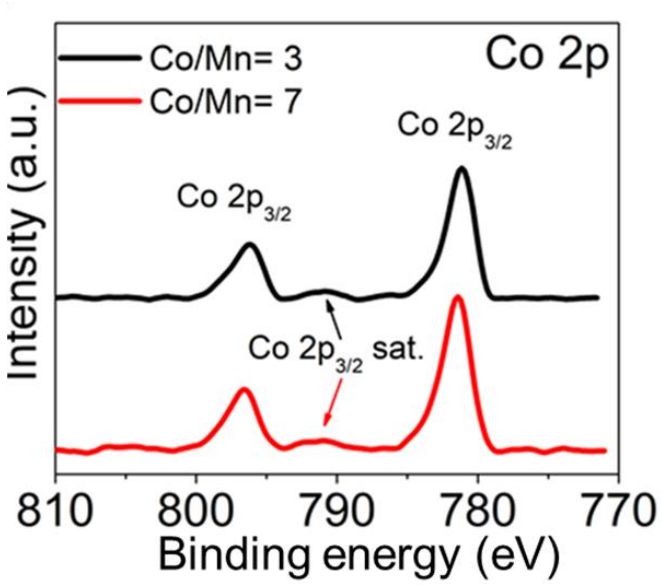

Figure S-11: (a) The UV-vis spectra of $CMOH_{acetate}$ deposited under varied deposition time at 80°C. (b) The corresponding calibration curve of (a) with 550-nm absorbance.

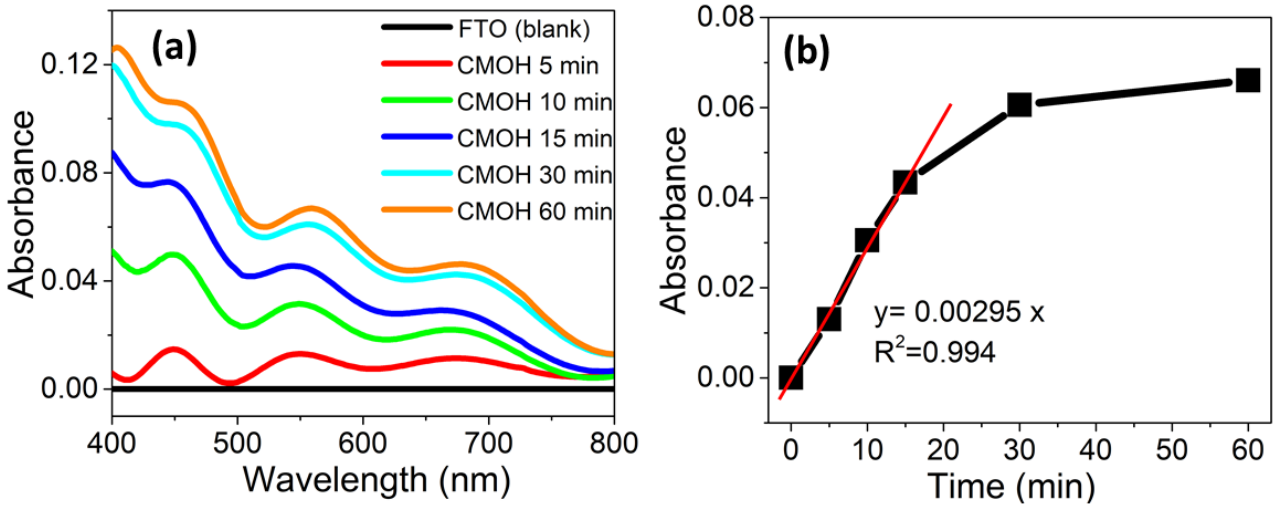

Figure S-12: The characterization of amorphous iron manganese oxide and ternary iron cobalt manganese oxide coatings on SiO_2/Si wafers. The SEM results reveal that both these two coatings (iron manganese oxides in (a) and iron cobalt manganese oxide in (b)) are highly smooth and crack-free. Their EDXS results are shown in (c) and (d), respectively, giving the corresponding compositions of Fe:Mn=2.39:1 and Fe:Co:Mn=1:2.11:0.77. The insets in (a) and (b) shows the photographs of the film appearance on FTO.

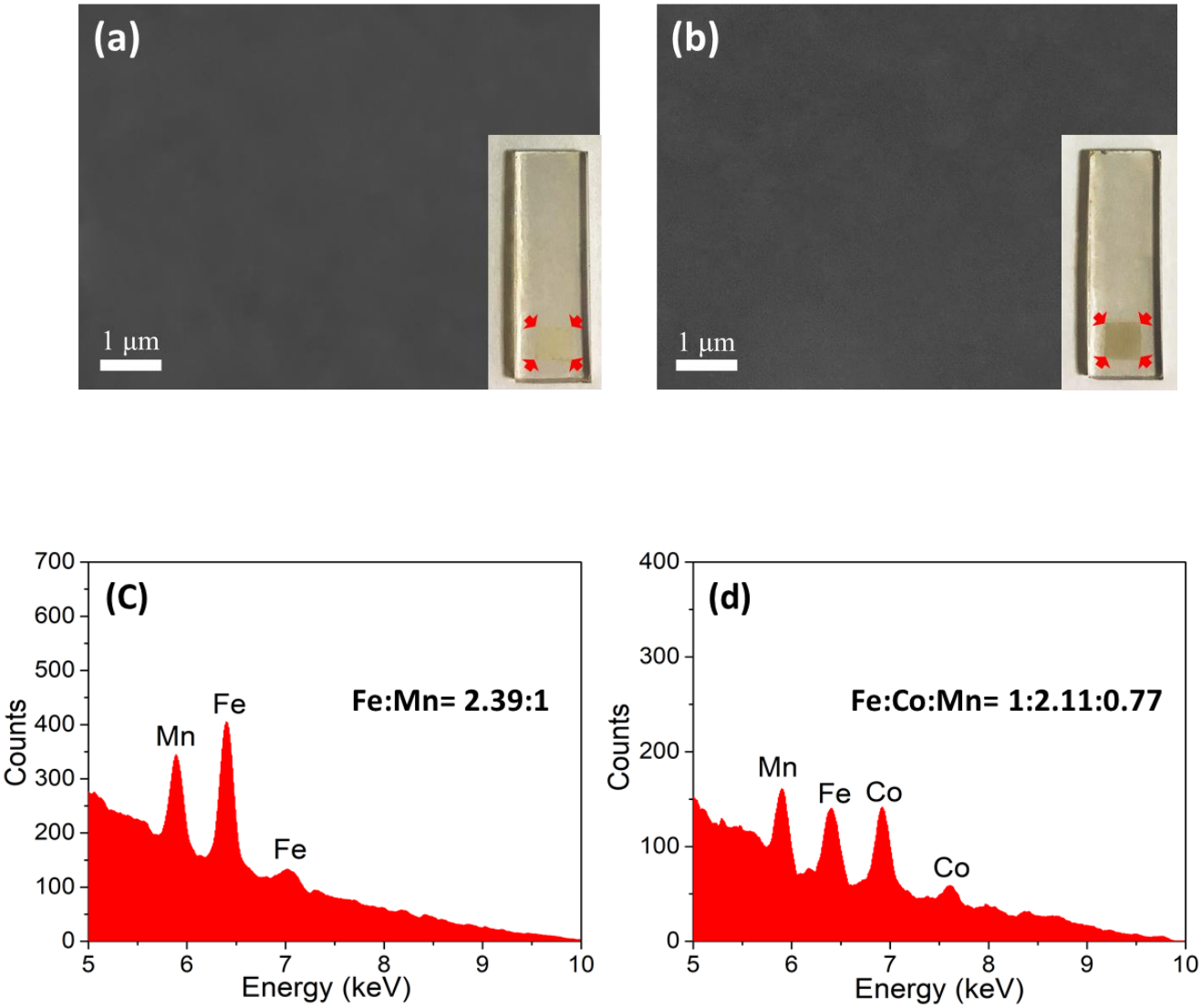

Table S-1: The OER performance comparison between $CMOH_{acetate}$ and the reported electrocatalysts.

Sample	Onset potential (V)	Potential @10 mA cm^{-2}	Electrolyte	Reference
CoPi	1.64	N/A	0.1 M KPi	1
$Ni_{0.9}Fe_{0.1}O_x$	1.53	1.57	1 M KOH	2
Mn_2O_3	N/A	1.81	0.1 M KOH	3
$FeCoNiO_x$	1.42	N/A	0.1 M KOH	4
$Fe_{40}Co_{40}Ni_{20}O_x$	1.42	N/A	0.1 M KOH	5
Mn_2O_3	1.40	1.67[a]	1 M KOH	6
Mn/Co-CB	1.45	N/A	0.1 M KOH	7
CoO_x–CoSe	1.50	N/A	1 M KOH	8
Cu_3P	1.60	N/A	0.1 M KOH	9
CMOH	1.28	1.62	0.1 M KOH	This work

[a] Estimated based on the reported OER results.

Reference:

1. M. W. Kanan and D. G. Nocera, *Science*, 2008, **321**, 1072-1075.
2. L. Trotochaud, J. K. Ranney, K. N. Williams and S. W. Boettcher, *J. Am. Chem. Soc.*, 2012, **134**, 17253-17261.
3. K. L. Pickrahn, S. W. Park, Y. Gorlin, H.-B.-R. Lee, T. F. Jaramillo and S. F. Bent, *Adv. Energy Mater.*, 2012, **2**, 1269-1277.
4. R. D. L. Smith, M. S. Prévot, R. D. Fagan, Z. Zhang, P. A. Sedach, M. K. J. Siu, S. Trudel and C. P. Berlinguette, *Science*, 2013, **340**, 60-63.
5. R. D. L. Smith, M. S. Prévot, R. D. Fagan, S. Trudel and C. P. Berlinguette, *J. Am. Chem. Soc.*, 2013, **135**, 11580-11586.
6. A. Ramírez, P. Hillebrand, D. Stellmach, M. M. May, P. Bogdanoff and S. Fiechter, *J. Phys. Chem. C*, 2014, **118**, 14073-14081.
7. E. Davari, A. D. Johnson, A. Mittal, M. Xiong and D. G. Ivey, *Electrochim. Acta*, 2016, **211**, 735-743.
8. X. Xu, P. Du, Z. Chen and M. Huang, *J. Mater. Chem. A*, 2016, **4**, 10933-10939.
9. C.-C. Hou, Q.-Q. Chen, C.-J. Wang, F. Liang, Z. Lin, W.-F. Fu and Y. Chen, *ACS Appl. Mater. Interfaces*, 2016, **8**, 23037-23048.